Dyes and Pigments 199 (2022) 110105

Contents lists available at ScienceDirect

Dyes and Pigments

journal homepage: www.elsevier.com/locate/dyepig

Intramolecular charge transfer and molecular flexibility: Key parameters to be considered in the design of highly fluorescent *p*-phenylene vinylene derivatives

Pedro J. Pacheco-Liñán [a], Amparo Navarro [b,**], Juan Tolosa [c,d], Mónica Moral [e], Cristina Martín [a,d,f], Iván Bravo [a,d], Johan Hofkens [f], Joaquín C. García-Martínez [c,d,***], Andrés Garzón-Ruiz [a,*]

[a] Department of Physical Chemistry, Faculty of Pharmacy, University of Castilla-La Mancha, C/ José María Sánchez Ibañez s/n, 02071, Albacete, Spain
[b] Department of Physical and Analytical Chemistry, Faculty of Experimental Sciences, Universidad de Jaén. Campus Las Lagunillas, 23071, Jaén, Spain
[c] Department of Inorganic, Organic Chemistry and Biochemistry, Faculty of Pharmacy, University of Castilla-La Mancha, C/ José María Sánchez Ibañez s/n, 02071, Albacete, Spain
[d] Regional Center for Biomedical Research (CRIB), C/ Almansa s/n, 02071, Albacete, Spain
[e] Renewable Energy Research Institute, University of Castilla-La Mancha, Paseo de la Investigación 1, 02071, Albacete, Spain
[f] KU Leuven, Leuven Chem&Tech - Molecular Imaging and Photonics (MIP), Celestijnenlaan 200F post box 2404, 3001, Leuven, Belgium

ARTICLE INFO

Keywords:
1,3,5-tristyrylbenzene
Intramolecular charge transfer
Photoisomerization
OLED
fluorescence spectroscopy
DFT calculations

ABSTRACT

The optoelectronic properties of a series of *p*-phenylene vinylene derivatives are studied herein to scrutinize their relationship with the molecular flexibility of the peripheral groups induced by the hybridization of the presented nitrogen atoms. All the molecules share a model fluorophore in the core, 1,3,5-tristyrylbenzene, as a structural leitmotif, while TPA and carbazole groups are located in the periphery. The studied compounds showed high luminescence, highlighting the TPA derivative (compound **1**) with a fluorescence quantum yield of 91% in dichloromethane solution. In addition, a linear relationship between the fluorescence lifetime and the solvent polarity was found for this compound. The solvent dependence was associated with an intramolecular charge transfer (ICT) upon photoexcitation which leads to a large change of the dipole moment and geometrical modifications mainly involving a single branch of the molecule. The photophysical properties of the carbazole derivatives (compounds **2** and **3**) are strongly influenced by the substitution position of the peripheral carbazole groups (C–N or C–C linkage, respectively). Interestingly, a linear relationship between the non-radiative rate constant and the solvent viscosity was found for compound **3**. This behavior was associated to the higher rigidity of this compound because the carbazole groups are embedded in the branches of the molecule and not in a terminal position as in compound **2**. Finally, the three studied compounds were used as electroluminescent material for non-doped OLEDs (organic light emitting diodes) in a proof-of-concept. This experiment also showed the importance of the molecular packing for having a good device performance.

1. Introduction

Aryl amines, especially triphenylamine (TPA) and carbazole, have been widely used as electron donor groups to modulate the electronic properties of many molecular systems because of their low cost of the reagents, easy structural tunability, good thermal stability, good hole-transport properties, ease of oxidation, interesting radical photoinitiating properties, strong intramolecular charge transfer (ICT), among others [1–4]. All these properties make them an important type of organic compounds for optoelectronic applications such as organic light emitting devices (OLED), dye-sensitive solar cells (DSSCs), or nanosecond lasers [2,5] [–] [8].

The electron-donating ability of the TPA and carbazole is due to the lone pairs of the nitrogen atom which is bound to several phenyl rings.

* Corresponding author. Faculty of Pharmacy, University of Castilla-La Mancha, C/ José María Sánchez Ibañez s/n, 02071, Albacete, Spain.
** Corresponding author. Faculty of Experimental Sciences, Universidad de Jaén. Campus Las Lagunillas, 23071, Jaén, Spain.
*** Corresponding author. Faculty of Pharmacy, University of Castilla-La Mancha, C/ José María Sánchez Ibañez s/n, 02071, Albacete, Spain.
E-mail addresses: anavarro@ujaen.es (A. Navarro), joaquinc.garcia@uclm.es (J.C. García-Martínez), andres.garzon@uclm.es (A. Garzón-Ruiz).

https://doi.org/10.1016/j.dyepig.2022.110105
Received 16 November 2021; Received in revised form 15 January 2022; Accepted 16 January 2022
Available online 21 January 2022

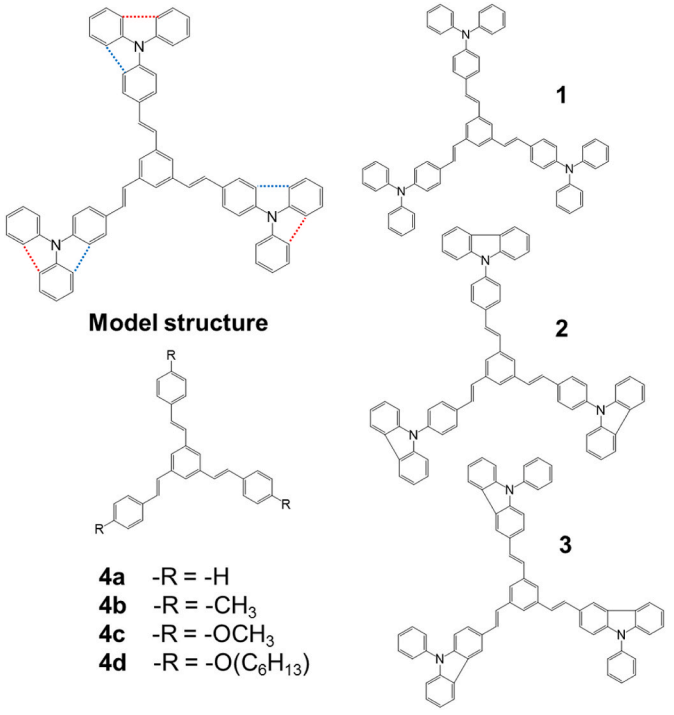

Scheme 1. Chemical structure of molecules **1**–**3** along with some related compounds (**4a**, **4b** and **4c**). Model structure shows the interring C–C bonds that differentiate the studied molecules.

Nevertheless, the linking to form a five-membered ring in the carbazole gives rise to structural characteristics that strongly affect the final electronic properties of the molecule. Carbazole is planar and leads to a more effective overlap of the π-orbitals, whereas the free rotation of the phenyl rings in the TPA has been employed as an inducer of restriction of intramolecular motions (RIM) in molecules exhibiting aggregation induced emission (AIE) properties [9] [–] [11]. However, despite the similarities and differences between the two groups, there are not many studies on how this structural difference affects the ultimate photoluminescent properties [12] [–] [14]. Thus, one of the main aims of the present work is to study the effect of both groups on the optoelectronic properties of a model fluorophore, i.e. 1,3,5-tristyrylbenzene (compound **4a** in Scheme 1). The selected fluorophore has been used as a model structure in diverse photophysical studies because its optical properties are modulated by the functional groups that decorate this scaffold [15] [–] [20]. The derivative **4d** has also proven to be suitable for fabricating optoelectronic devices [21,22].

In a previous work, excellent luminescent properties (with quantum yields, Φ_F, within 59–83%) were reported for a compound formed by a core of 1,3,5-tristyrylbenzene and peripheral carbazole groups (compound **2** in Scheme 1) [16]. Starting from these promising results, we here compare the optoelectronic properties of compounds **1** and **3** with **2**, where the only structural difference is the presence or absence of the interring C–C bonds (dotted line in Scheme 1). All these molecules share 1,3,5-vinylbenzene as a common motif while the peripheral moieties are different, i.e. molecule **1**, without any (dotted line) interring bond, is decorated with three triphenylamine (TPA) groups in the periphery [23]; carbazoles are the peripheral groups of **2** and are linked to 1,3,5-tristyrylbenzene core through C–N bonds [16]; on the contrary, carbazole groups have a more central location in the molecular structure of **3** while phenyl rings occupy the terminal position of each branch (as we are aware, this compound has been synthesized for the first time in this work). Despite the structural similarity between the three compounds, the apparent differences between TPA and carbazole and the different way of anchoring of the latter confers different final optoelectronic properties to the molecule. In addition, the presence of TPA and carbazole groups in the periphery of the molecule leads to intramolecular charge transfer (ICT) upon photoexcitation [16]. As will be discussed, ICT processes also have a significant impact on photophysical properties of some of these compounds. Finally, they were employed as electroluminescent materials for the fabrication of non-doped OLEDs.

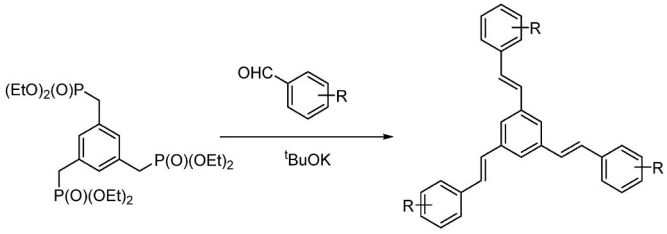

Scheme 2. Synthesis of compounds **1** and **3**.

2. Materials and methods

2.1. General

All reagents were used as received and without further purification. Toluene (Tol), tetrahydrofuran (THF), dichloromethane (DCM), acetonitrile (ACN), dimethylsulfoxide (DMSO) and glycerol were used as CHROMASOLV quality. In air- and moisture-sensitive reactions, all glassware was flame-dried and cooled under argon.

2.2. Synthesis

Formation of the double bonds in compounds **1** and **3** was performed by the reaction of a commercial aldehyde with hexaethyl(benzene-1,3,5-triyltris(methylene))tris(phosphonate) in the presence of potassium *tert*-butoxide, a standard methodology for the Horner−Wadsworth−Emmons reaction (Scheme 2). Specific details concerning preparation of **1** and **3** and their characterization are provided in the Supporting Information.

2.3. Spectroscopic experiments

Spectra were acquired in different solvents at 20 °C and sample concentration of 1 μM. Quartz cuvettes (Hellma Analytics) of 10 mm were employed for all the UV–Vis absorption and fluorescence emission measurements of liquid samples.

UV–Vis absorption spectra were recorded in a V-750 (Jasco) spectrophotometer using a slit width of 0.4 nm and a scan rate of 600 nm min^{-1}. A Peltier accessory was employed to control the temperature of the spectrophotometer measuring cell.

Steady-state and time-resolved fluorescence spectroscopy (SSFS and TRFS, respectively) experiments were recorded on a FLS920 spectrofluorometer (Edinburgh Instruments) equipped with a MCP-PMT (microchannel plate-photomultiplier tube) detector (R3809 model) and a TCSPC (time-correlated single photon counting) data acquisition card (TCC900 model). A Xe lamp of 450 W was used as the light source and the excitation for SSFS measurements and a EPLED360 subnanosecond pulsed light emitting diode (Edinburgh Photonics) was employed as light source at 368 nm for TRFS experiments. A TLC 50 temperature-controlled cuvette holder (Quantum Northwest) was employed for SSFS and TRFS measurements.

The fluorescence intensity decays, $I(t)$, were fitted by using an iterative least-square fit method to the following multiexponential function:

$$I(t) = \sum_{i=1}^{n} \alpha_i \exp(-t/\tau_i) \quad (1)$$

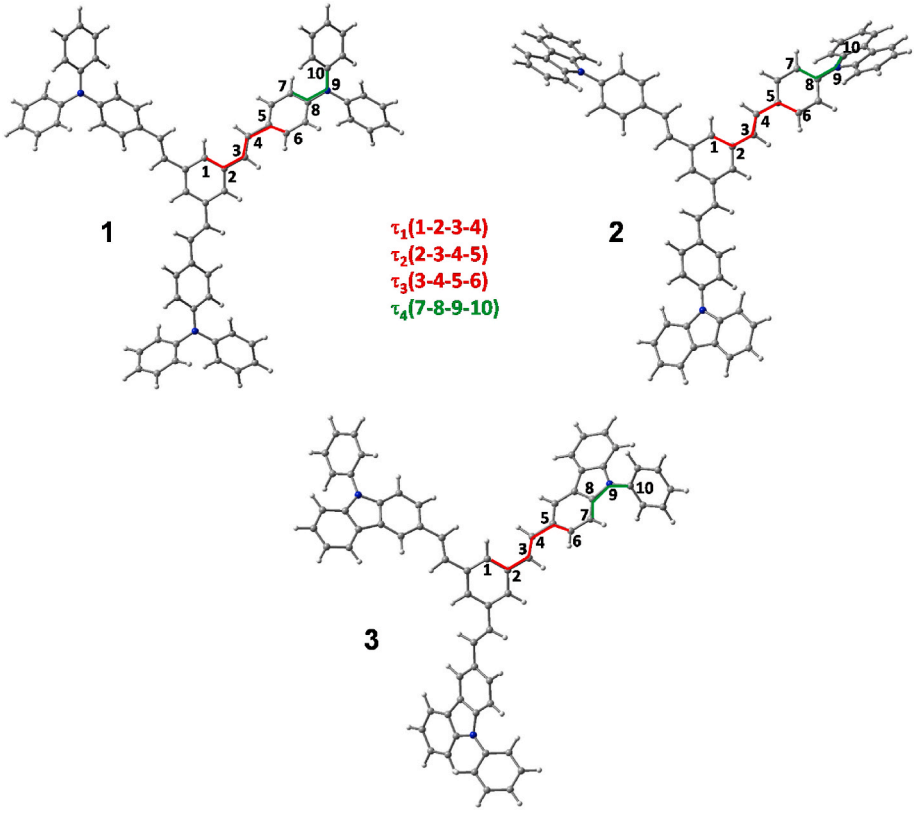

Fig. 1. Molecular structure of compounds **1**, **2** and **3** calculated at the M06-2X/6-31G* level of theory using dichloromethane as solvent. The numbering and dihedral angles τ_1 – τ_4 are used in Fig. 1, S1 and Table S1 are shown.

where α_i and τ_i are the amplitude and lifetime for each *i*th term. The mean decay lifetime (τ_m) was then calculated as:

$$\tau_m = \frac{\sum_{i=1}^{n} \alpha_i \tau_i^2}{\sum_{i=1}^{n} \alpha_i \tau_i} \quad (2)$$

Quantum yields were measured in a FS5 spectrofluorometer (Edinburgh Instruments) equipped with an integrating sphere, a 150 W Xe lamp as the light source and a PMT (photomultiplier tube) detector (R928P model). Quantum yield calculations were carried out using the F980 Software of Edinburgh Instruments.

2.4. OLED device fabrication

An indium-tin-oxide (ITO)-coated glass (~109 Ω cm) was used as substrate. Before use, the glass was washed by immersion and sonication for 10 min in following solvents: 1) alkaline-detergent water (Hellmanex solution), water, acetone and isopropanol. The cleaned ITO-glasses were treated in an ultraviolet-ozone reactor (30 min) to lower the work function of the ITO layer. After that, a solution of the hole-injection layer, poly(3,4-ethylenedioxythiophene):polystyrene (PEDOT:PSS; Sigma Aldrich, high conductivity), was spin coated at 3000 rpm for 120 s and subsequently annealed at 150 °C during 15 min. Next, a 5 mg mL^{-1} solution of the selected carbazoles in acetonitrile (Sigma Aldrich, anhydrous), was spin coated for 60 s at 1000 rpm and annealed at 80 °C for 15 min. Finally, a 150 nm aluminum (Al) electrode layer was vapor deposited on top of the emissive layer.

Stationary electroluminescence measurements were recorded using an Edinburgh FLS 980 fluorimeter where the Xe-lamp (usually for optical excitation) was blocked in order to only register the electroluminescence spectra. Current – Voltage (I–V) curves were measured in the dark at room temperature using a Keithley 2400 device.

2.5. Computational details

Full geometry optimizations were performed using the Gaussian09 (revision D.01) suite of programs [24] at the M06-2X/6-31G* level of theory [25]. We chose the meta-hybrid M06-2X functional because, in previous studies, it has provided a reasonable accuracy in the calculation of photophysical properties of 1,3,5-tristyrylbenzene derivatives [15–17,26]. The molecular geometries of the ground state, S_0, and the first excited state, S_1, were optimized and the vibrational modes were calculated to check the absence of imaginary frequencies. The solvent environment was described by the polarizable continuum model (PCM) as implemented in the Gaussian package [27] [–] [29]. The vertical electronic transitions (absorption and emission) were computed using time dependent (TD)-DFT (TD-M06-2X/6-31G*). The fluorescence emission energy in solution was calculated as

$$\Delta E_{em} = E_{S1}(G_{S1}) - E_{S0}(G_{S1}) \quad (3)$$

where $E_{S1}(G_{S1})$ is the energy of the S_1 state at its equilibrium geometry (state-specific solvation approach) [30] and $E_{S0}(G_{S1})$ is the energy of the S_0 state at the S1 state geometry and with the static solvation from the excited state [31].

The reorganization energy, λ, associated to the electronic relaxation was calculated using the DUSHIN program [32] according to:

$$\lambda = \sum_i \lambda_i = \sum_i \hbar \omega_i S_i \quad (4)$$

where ω_i is the wavenumber associated to the vibrational mode *i*, and S_i is the Huang-Rhys (HR) parameter calculated from the atomic displacements ΔQ and force constant, *k*, of the normal mode *i* according to

$$S_i = \frac{1}{2} k \frac{\Delta Q^2}{\hbar \omega_i} \quad (5)$$

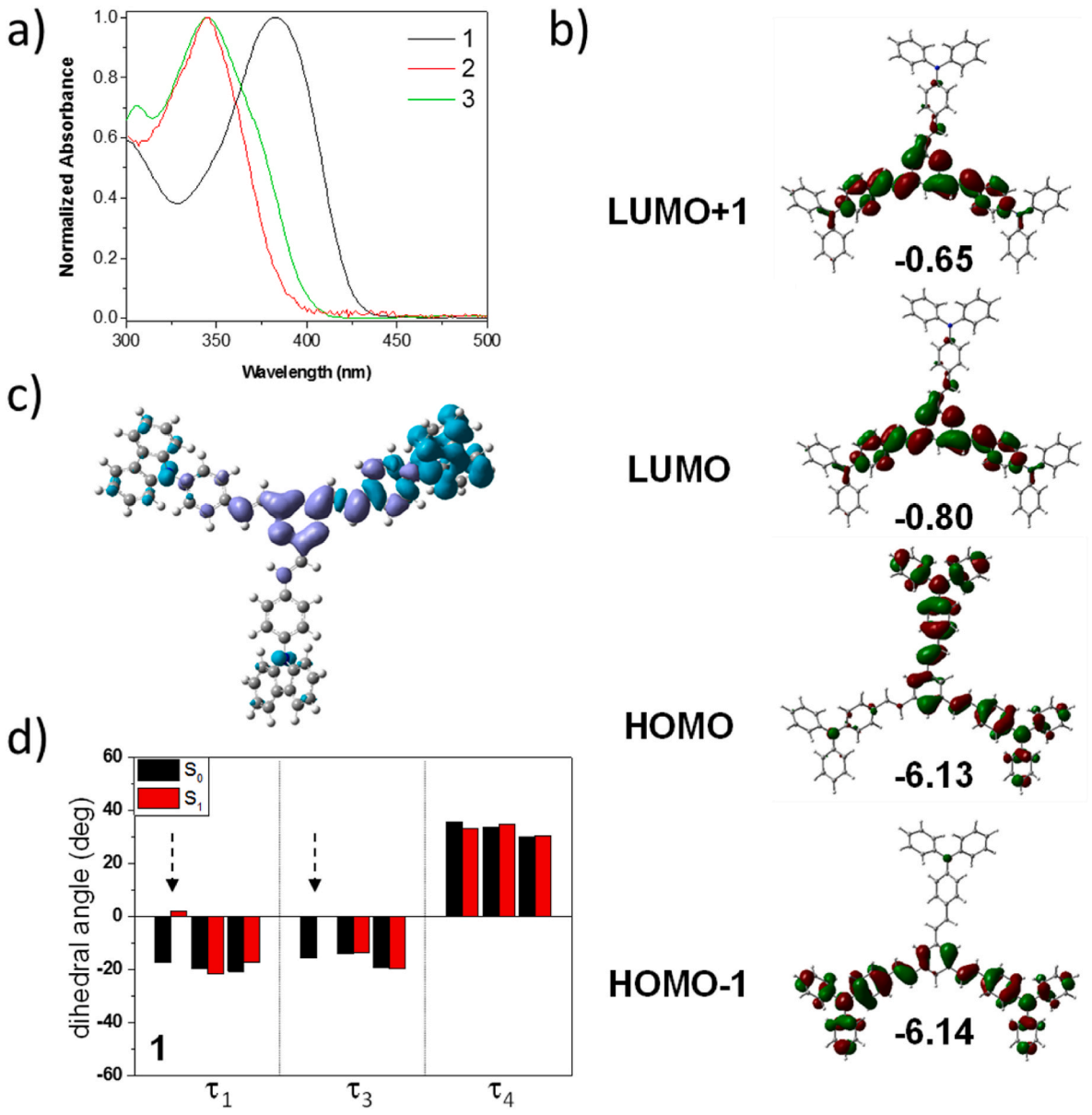

Fig. 2. (a) Normalized absorption spectra of compounds **1**–**3** in dichloromethane solution (sample concentrations were 1 μM) [2]. (b) Isocontour plots (0.02 au) of some selected frontier molecular orbitals of **1** (and their energy levels in eV) in dichloromethane solution computed at the M06-2X/6-31G* level of theory. (c) Charge density distribution (hole in green; electron in purple) calculated for **1** in S_1 state (TD-M06-2X/6-31G*, dichloromethane solution). (d) Some selected dihedral angles (τ_1, τ_2 and τ_4 of each branch of the molecule) calculated for the S_0 and S_1 states of **1** in dichloromethane (the arrows indicate significant changes). (For interpretation of the references to color in this figure legend, the reader is referred to the Web version of this article.)

The quantitative indicator of the charge-transfer length (Δr) was calculated as proposed by Adamo et al., [33].

3. Results and discussion

The molecular structure of **1**–**3** was optimized in dichloromethane solution at the M06-2X/6-31G* level of theory. The planarity of 1,3,5-trivinylbenzene core is affected by the presence of TPA or carbazole groups in the periphery of the molecule. Typically, 1,3,5-tris(styryl)benzene derivatives (**4**) have slightly twisted branch geometries resembling fan blades. Instead, the core of molecule **2** is near-planar while dihedral angles $|\tau_1|$ and $|\tau_3|$ reach values up to 24° and 14°, respectively, for compound **3** (see Fig. 1 and S2, and Table S1). Nevertheless, the lowest bond length alternation, BLA, value (0.127), associated to a more efficient conjugation, was found for the core of **1** (see Table S1). A distinct scenario was observed in the peripheral groups, being especially interesting the differences observed between molecules **1** and **2**. The existence of the interring bond (marked with dotted line) brings on a twisting of the peripheral groups, i.e. $|\tau_4|$ is within 30-36° for TPA groups of compound **1** while $|\tau_4|$ increases up to 51-52° for the carbazole moieties of compound **2**. The terminal phenyl rings of compound **3** are also highly twisted with respect to the carbazole group ($|\tau_4|$ = 52-53°).

Fig. 2a shows the absorption spectra recorded for compounds **1**–**3** in dichloromethane solution (see Fig. S4, as well as Table 1 and S2 for additional spectra and details) [2]. In general, the lowest-energy absorption band of these compounds was not very sensitive to the polarity of the solvent. Considering dichloromethane as the reference solvent, the highest maximum absorption wavelength (λ_{ab}^{max}) was found for molecule **1** (383 nm), which is in accordance with its smaller BLA in the core and lower twisting of the peripheral groups (it is well-known that there is a close connection between the BLA and the electronic gap in conjugated oligomers) [34–36]. The lowest-energy absorption bands of

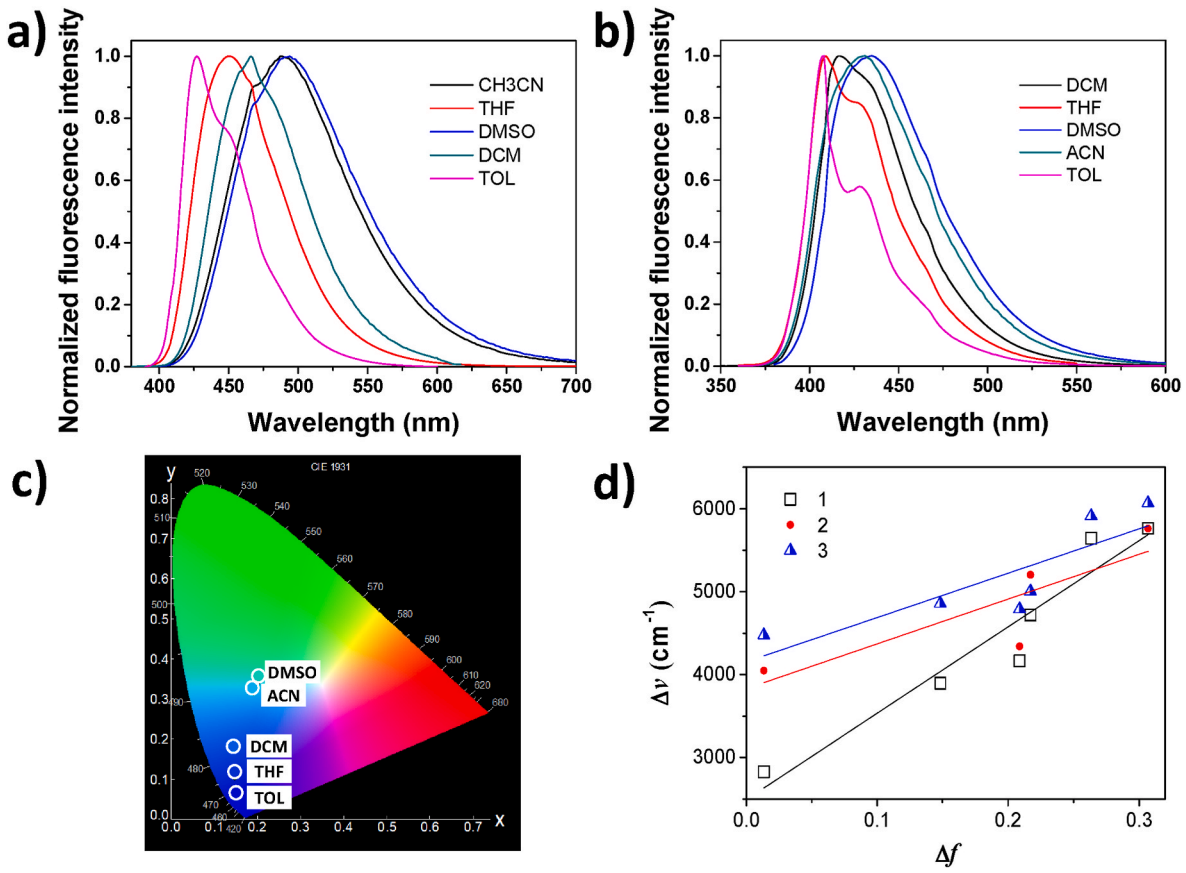

Fig. 3. Normalized fluorescence emission espectrum of compounds **1** (a) and **3** (b) in different solvents. (c) CIE1931 chromaticity diagram of solutions of compound **1** in different solvents. (d) Stokes shift ($\Delta\nu$) vs. Lippert−Mataga solvent polarity parameter (Δf) for compounds **1**–**3** (data corresponding to compound **2** were extracted from reference) [16].

the carbazole derivatives are centered at 343–344 nm being red-shifted with respect to the equivalent bands of the reference compound (1,3,5-tristyrylbenzene) and its methyl and methoxy derivatives (λ_{ab}^{max} is 317 nm for **4a**, 319–320 nm for **4b** and 327–328 nm for **4c** in dichloromethane solution) [19,37]. These results show the strong influence of the peripheral groups on the photophysical properties of 1,3,5-tristyrylbenzene derivatives. As discussed in previous works, the frontier molecular orbitals of 1,3,5-tristyrylbenzene derivatives were not uniformly distributed on all the branches of the conjugated core, leading to quasi-degenerate molecular orbitals and very close energies for the transitions $S_0 \rightarrow S_1$ and $S_0 \rightarrow S_2$ ($\Delta\lambda_{ab}^{calc} \leq 7$ nm) [15,16] (see Fig. 2b and S3). The main components of these transitions in compound **1** involve occupied molecular orbitals (HOMO, HOMO-1 and HOMO-2) predominantly localized on the external part of the molecule, including the TPA groups, while the unoccupied molecular orbitals (LUMO, LUMO+1 and LUMO+2) are particularly located on the central core. Therefore, $S_0 \rightarrow S_1$ and $S_0 \rightarrow S_2$ transitions have ICT character and similar conclusions can be obtained for the carbazole derivatives, i.e. **2** and **3** [16]. The ICT character of the $S_0 \rightarrow S_1$ transition can be quantitatively analyzed through the Δr index, proposed to measure charge transfer length during electron excitation [33]. Although the highest Δr index was obtained for compound **1** (3.62 Å), a comparable value was found for the carbazole derivative **2** (3.47 Å). On the other hand, compound **3** showed a significant smaller ICT character ($\Delta r = 2.54$ Å) than **2** mainly due to the position of the carbazole groups, more embedded in the core of the molecule and not totally located at the periphery. Therefore, if an ICT character is desired in the ultimate properties of the fluorophore, the carbazole unit should preferably be attached by the free nitrogen, as in compound **2**, rather than through one of the phenyls configuring the carbazole tricycle, as in compound **3.**

These ICT transitions also lead to interesting modifications of the molecular structure which mainly involve a single branch of the core of the molecule. In this sense, Fig. 2c shows how the hole charge density of molecule **1** in S_1 state is mainly located on the 1,3,5-trivinylbenzene central moiety but the electron charge density is placed on the TPA group of a single branch. In this branch, $|\tau_1|$ varies from 17° in the S_0 state to 2° in the S_1 state (see Fig. 2d and S2, and Table S1). Thus, $|\tau_3|$ varies from 16° to 0° upon the excitation and BLA drops from 0.127 to 0.007 in the same branch. On the contrary, the changes in the rest of the branches are comparatively small. The planarization of a branch of the core in the S_1 state was also observed for compound **2** [16] and, in less extension, for **3** ($|\tau_1|$ and $|\tau_3|$ did not drop below 5° and 3°, respectively, for this molecule). The worse planarization observed for **3** could be associated to the smaller ICT character of the $S_0 \rightarrow S_1$ transition as well as a higher molecular rigidity (because of the less peripheral position of the carbazole groups) with respect to compounds **1** and **2**.

Fine vibronic structure was partially observed for all the compounds fluorescence emission spectra recorded in low-polarity solvents such as toluene and tetrahydrofuran [16] (see Fig. 3a and b). On the contrary, vibronic structure was reported for the reference compound **4d** both in low-polarity solvents (*n*-hexane and tetrahydrofuran) and in a polar solvent as acetonitrile [17]. Therefore, the presence of carbazole and TPA groups seems to produce a certain distortion of the molecular symmetry in comparison to the reference structure. The fluorescence emission wavelength maximum (λ_{em}^{max}) of the studied compounds is sensitive to the solvent polarity and the Stokes shift is particularly large for **1** (see Table 2 and S4). The emission color of that compound can be tuned from blue to green as a function of the polarity of the solvent (Fig. 3c) while the fluorescence emission color of both carbazole derivatives is always blue. The influence of the solvent on the dipole

Table 1
Experimental maximum absorption wavelength (λ_{ab}^{max}) along with their molar absorption coefficients (ε) determined in dichloromethane solution. Calculated lowest-energy transition wavelengths (λ_{ab}^{calc}), oscillator strengths (f) and orbital contributions for these transitions. Calculations were carried out at the TD-M06-2X/6-31G* level of theory in dichloromethane solution.

Comp.	λ_{ab}^{max} (nm [eV])	$\varepsilon\pm2\sigma$ (cm mM^{-1})	λ_{ab}^{calc} (nm [eV])	f	Transition	Main component of the transition (≥20% contribution)
1	383 [3.24]	13.6 ± 4.0	349 [3.55]	1.81	$S_0\rightarrow S_1$	H-2→L+1(20), H→L(27)
			345 [3.59]	2.35	$S_0\rightarrow S_2$	H-2→L(27), H-1→L+2(21)
2	344 [3.60][a]	40.3 ± 3.4	329 [3.77]	1.71	$S_0\rightarrow S_1$	H-7→L(47), H-1→L(26)
			323 [3.84]	2.37	$S_0\rightarrow S_2$	H-2→L(20), H→L(20)
3	343 [3.61]	113.7 ± 2.2	322 [3.85]	1.61	$S_0\rightarrow S_1$	H→L(29)
			315 [3.94]	2.54	$S_0\rightarrow S_2$	H-2→L(22), H→L(24)

[a] From reference [16].

Table 2
Maximum excitation and emission wavelength (λ_{ex}^{max} and λ_{em}^{max}) recorded for compounds **1**–**3** in different solvents along with the wavelength calculated for the $S_1\rightarrow S_0$ transition (λ_{em}^{calc}) in dichloromethane solution. In addition, fluorescence quantum yield (Φ_F), mean fluorescence lifetime (τ_m), radiative rate constant (k_F) and non-radiative deactivation rate constant (k_{NR}) obtained in different solvents at 298 K are also collected.

Compd (solvent)[a]	λ_{ex}^{max} (nm [eV])	λ_{em}^{max} (nm [eV])	λ_{em}^{calc} (nm [eV])	Φ_F (%)	τ_F (ns)	k_F (ns^{-1})	k_{NR} (ns^{-1})
1 (Tol)	384 [3.23]	427 [2.90]		84	1.51	0.56	0.11
1 (THF)	377 [3.29]	450 [2.75]		82	2.00	0.41	0.09
1 (DCM)	383 [3.24]	466 [2.66]	442 [2.80]	91	2.37	0.38	0.04
1 (ACN)	377 [3.29]	480 [2.58]		87	4.01	0.22	0.03
1 (DMSO)	383 [3.24]	487 [2.55]		77	5.01	0.15	0.05
2 (Tol)	347 [3.57][b]	401 [3.09][b]		59[b]	3.41[b]	0.17[b]	0.12[b]
2 (THF)	343 [3.61][b]	403 [3.08][b]		80[b]	4.56[b]	0.18[b]	0.04[b]
2 (DCM)	345 [3.59][b]	419 [2.96][b]	408 [3.04]	75[b]	3.39[b]	0.22[b]	0.07[b]
2 (ACN)	341 [3.64][b]	429 [2.89][b]		83[b]	3.84[b]	0.22[b]	0.04[b]
3 (Tol)	344 [3.60]	408 [3.04]		60	3.44	0.17	0.12
3 (THF)	341 [3.63]	409 [3.03]		58	4.03	0.14	0.10
3 (DCM)	343 [3.61]	417 [2.97]	398 [3.12]	52	3.44	0.15	0.14
3 (ACN)	341 [3.63]	430 [2.88]		47	4.22	0.11	0.13
3 (DMSO)	345 [3.59]	435 [2.85]		67	4.54	0.15	0.07

[a] Tol, THF, ACN, DCM and DMSO are the used solvents: toluene, tetrahydrofuran, acetonitrile, dichloromethane and dimethyl sulfoxide.
[b] From reference [16].

moment upon excitation was studied through the Lippert-Mataga equation (see Supporting Information for details) [38] [–] [40]. The dependence of the Stokes shift versus Δf is shown in Fig. 3d. As expected, the highest slope in the Lippert-Mataga plot and the largest change in the dipole moment upon the excitation (μ_E-μ_G) were found for the TPA derivative **1** (21.1 D, see Tables S3 and S4 for details). Compound **1** exhibits Lippert-Mataga slope (LM slope = 1.04×10^4 cm^{-1}) and μ_E-μ_G value comparable or higher than those reported for other star-shaped molecules with a central TPA moiety and peripheral groups such as 2,3,3-triphenylacrylonitrile (LM slope of 1.39×10^4 cm^{-1}) [41], pyridine (μ_E-μ_G = 6.15 D) [42], thiophene (μ_E-μ_G = 6.55 D) [42] and thienothiophene (μ_E-μ_G = 7.68 D) [42], among others. On the other hand, the change in the dipole moment upon the excitation is similar in both carbazole derivatives (μ_E-μ_G is 14.1 D for **2** and 14.8 D for **3**) [16].

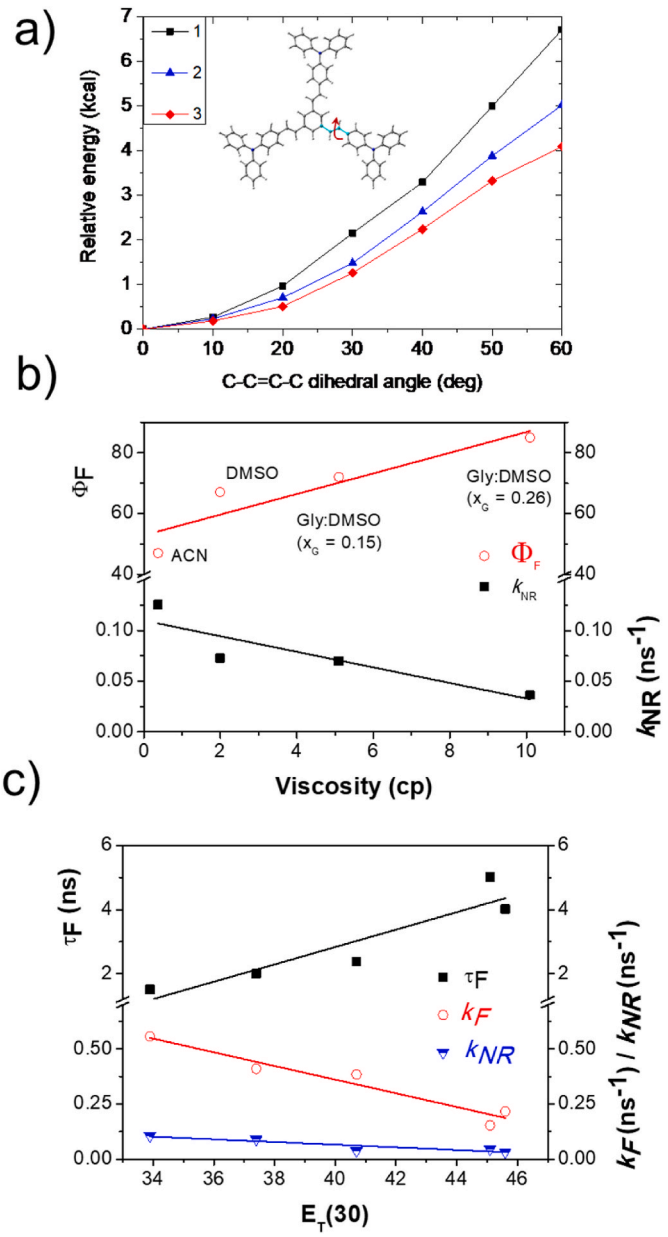

Fig. 4. (a) Torsional barriers around the vinylene moiety (τ_2) calculated for **1**–**3** in the S_1 excited state (dichloromethane solution). The zero level of energy corresponds to the full-trans configuration computed at the M06-2X/6-31G* level of theory. (b) Correlation of Φ_F and k_{NR} determined for **3** with respect to the solvent viscosity (ACN, η = 0.369 cp; DMSO, η = 1.987 cp; mixtures of Glycerol:DMSO, i.e. $x_{Glic.}$ = 0.15, η = 5.1 cp; $x_{Glic.}$ = 0.26, η = 10.1 cp) [48,49]. (c) Correlation of τ_F, k_F and k_{NR} determined for **1** with respect to the polarity parameter $E_T(30)$ (Tol, $E_T(30)$ = 33.9; THF, $E_T(30)$ = 37.4; DCM, $E_T(30)$ = 40.7; DMSO, $E_T(30)$ = 45.1; ACN, $E_T(30)$ = 45.6) [50].

The fluorescence quantum yields, Φ_F, and lifetimes, τ_F, determined for the studied compounds are shown in Table 2, along with the kinetics

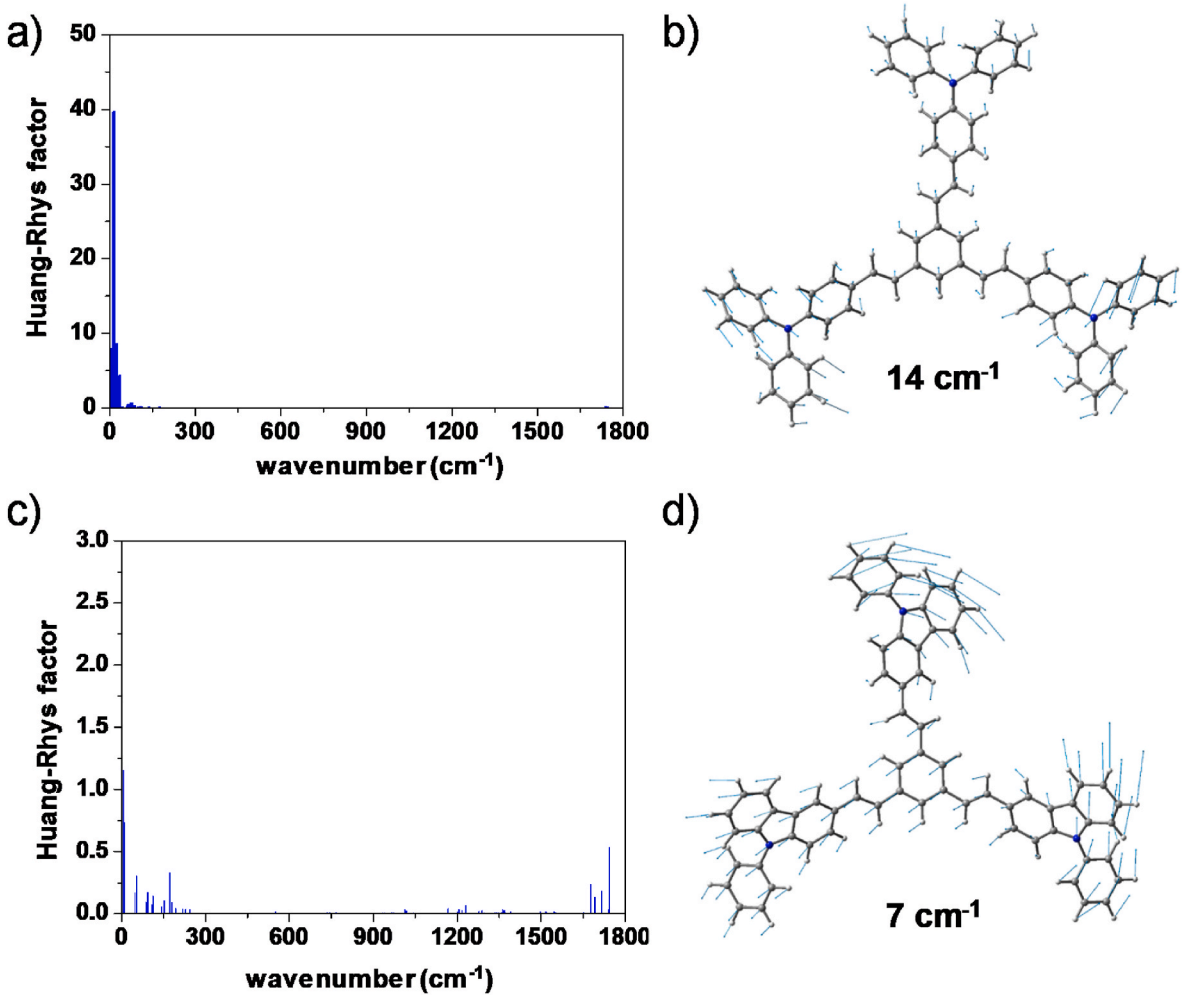

Fig. 5. (a) HR factors calculated for **1** vs. the normal modes of the ground state (M06-2X/6-31G*, dichloromethane solution). (b) The normal mode of **1** with the highest HR factor. (c) HR factors calculated for **3** vs. the normal modes of the ground state (M06-2X/6-31G*, dichloromethane solution). (d) The normal mode of **3** with the highest HR factor.

rate constants calculated for the radiative deactivation k_F and non-radiative deactivation, k_{NR} (see Supporting Information for details). The kinetics rate constants were calculated through

$$k_F = \Phi_F / \tau_F \quad (6)$$

$$\tau_F = 1 / (k_F + k_{NR}) \quad (7)$$

Internal conversion (IC), intersystem crossing (ISC) and *trans→cis* photoisomerization are some of the classical non-radiative deactivation mechanisms of the excited state of π-conjugated organic compounds. ISC from the S_1 state to the T_1 state can be neglected for 1,3,5-tristyrylbenzene derivatives because of the large energy gap between these states [16]. The non-radiative IC mechanism was analyzed through the Huang–Rhys (HR) factors which allow the identification of the vibrational modes involved in that process [43]. *Trans→cis* photoisomerization is also a contributing deactivation pathway of *trans*-stilbene derivatives [44] [–] [47]. The highest fluorescence quantum yields (≥77%) were determined for the TPA derivative while the lowest ones were measured for compound **3** (≤67%). Accordingly, the non-radiative rate constants calculated for **3** in different solvents are comparable or even higher than its radiative constants. The photoisomerization process was studied through the effect of the solvent viscosity on k_{NR} and the calculation of the *trans→cis* rotational barrier in the excited state. As shown in Fig. 4a, the lowest energy barrier around the vinylene bridge (τ_2) was computed for **3** and, hence, the photoisomerization should be a more efficient deactivation mechanism for this compound than for **1** and **2**. It is well-known that viscous media hinder the *trans-cis* photoisomerization increasing Φ_F [44] [–] [47]. Fig. 4b shows the positive linear correlation found between the quantum yield determined for **3** and the solvent viscosity (only polar solvents such as acetonitrile and dimethyl sulfoxide, and mixtures of dimethyl sulfoxide and glycerol were employed for this experiment). Accordingly, k_{NR} decreases as a function of the viscosity of the medium (see Fig. 4b). Nevertheless, the viscosity could also have an effect on the IC mechanism. One normal mode with a significant HR factor (1.2) was computed for **3** (see Fig. 5, S6 and S7, and Table S6). This mode corresponds to a wagging of the entire branches of the molecule, in contrast to the normal modes mainly responsible for IC deactivation of **2** which only involve to the peripheral carbazole groups. Thus, the size of the groups involved in those normal modes could determine the sensitivity of the IC mechanism to the solvent viscosity. A clear correlation between k_{NR} of **3** and the polarity of the solvent was not observed.

The highest k_F values were calculated for **1** in agreement with the large quantum yields determined for this compound. The Strickler–Berg relation establishes that the radiative rate constant is directly related to the oscillator strength [51,52]. Accordingly, the highest oscillator strength was computed for the transition $S_0 \rightarrow S_1$ of compound **1** as showed in Table 1. In addition, the highest *trans→cis* photoisomerization barriers were calculated for this compound. Consequently, the strong luminescence of this compound could also be associated with a low

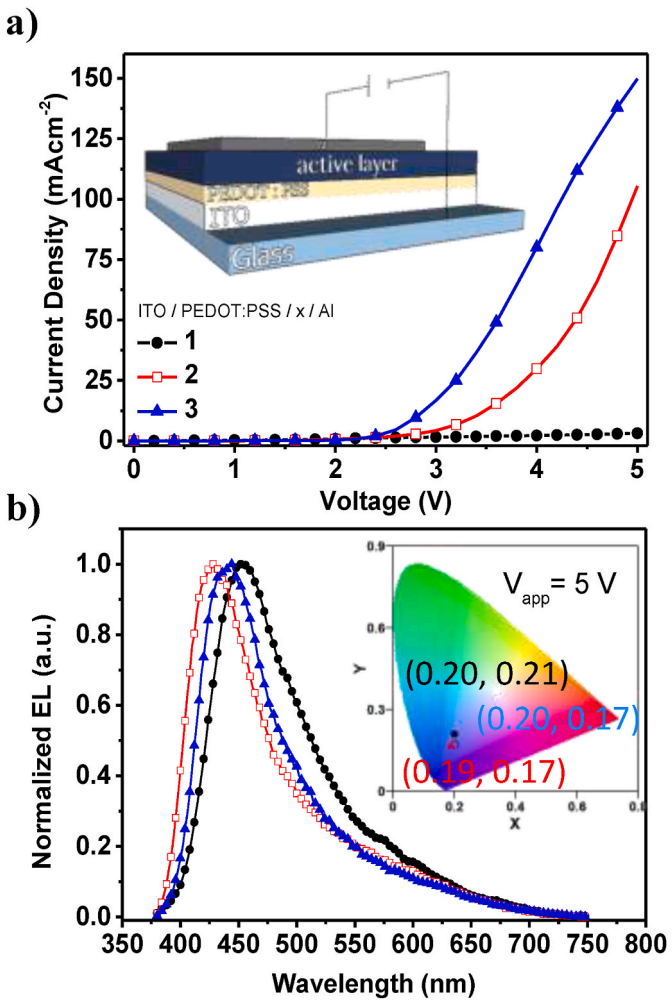

Fig. 6. (a) Current vs voltage curve and (b) electroluminescence spectra of the prepared OLED from compounds **1**–**3** at 5V. The inset in (a) shows a schematic representation of the OLED architecture. The inset in (b) shows the CIE coordinates obtained for each device.

efficiency of this non-radiative mechanism. In contrast, six normal modes with noticeable large HR factors (from 3.8 to 39.7) were found for **1**, in dichloromethane solution, suggesting that IC could be a main non-radiative deactivation pathway. In general, these frequencies correspond to wagging and rocking motions of the peripheral TPA groups (Fig. 5, S6 and S7, and Table S6). It was also observed that the polarity of the solvent has a strong influence on the fluorescence lifetime (from 1.51 ns in toluene to 5.01 ns in dimethyl sulfoxide) while the quantum yield remains between 77% and 91% (see Fig. 4c). In consequence, the lifetime of the excited state significantly increases in polar solvents, probably associated to the ICT process and the large change of the dipole moment of the molecule. As shown in Fig. 4c, k_F and k_{NR} decreases with the solvent polarity. Interestingly, we found that the highest HR factor calculated for **1** in toluene (35.6) and dichloromethane (39.7) dropped to half (16.1) in acetonitrile solution (Fig. S8). In summary, the ICT process, associated with the higher flexibility of the molecular structure of **1**, leads to a greater planarization of the core in the excited state, enhancing its fluorescence emission.

The strong luminescence of the studied compounds encouraged us to investigate their electroluminescent properties being incorporated in a light-emitting device as emissive layer. Previously, it was determined that compound **1** is chemically stable up to 200 °C and the carbazole derivatives up to 450 °C (see the thermogravimetric analysis in Figure S10). Thus, the thermal stability showed by all the studied compounds is suitable to be incorporated in OLEDs [53]. In a preceding work, the parent compound **4d** was used as an active layer in the fabrication of a OLED (ITO/PEDOT:PSS(75 nm)/active layer/Al) [22]. Similar single-layer devices were fabricated for the studied compounds here (ITO/PEDOT:PSS(40 nm)/active layer(~50 nm)/Al(150 nm); see the scheme in the inset of Fig. 6a). Their current-voltage curves showed typical diode characteristics [54]. Interestingly, the lowest turn-on voltages were found for the carbazole derivatives (~3 V for compound **2**; ~2 V for compound **3**; see Fig. 6a). These differences observed between carbazole and TPA derivatives could be associated with the different packing and intermolecular interaction in the solid state. The OLEDs fabricated with the carbazole derivatives also showed lower turn on voltages than the one using **4d** as active layer (9 V) [22]. For all the compounds, a good match between the electroluminescence (EL) and photoluminescence (PL) maxima (in acetonitrile solution) was found (Fig. 6b displays the EL spectra at 5 V). Nevertheless, a broadening of the EL bands with respect to the PL ones was observed. This is particularly notorious in the case of compound **3**, for which FWHM (full width at half maximum) is 3700 and 4300 cm^{-1} for PL and EL spectra, respectively. These differences are reflected in the CIE coordinates (see Table S5). Similar observations were reported for other amorphous layers and the main explanation is related to the intermolecular packing in the solid state which leads to a larger number of electron and hole traps [55]. To confirm this hypothesis, the UV–Vis absorption and PL spectra of the three studied compounds in thin film were recorded (see Fig. S9; thin films were prepared by spin coating from acetonitrile solutions on quartz plates). In all the cases, the absorption bands become broader and red shifted in comparison to those obtained in acetonitrile solution. The broadening is also observed for the PL spectra, while the maxima are located at the same position than in acetonitrile solution. This suggests that the molecules are mainly presented as monomers but the presence of shoulders (for instance at ~430 and 550 nm for compound **3**) could be related to the formation of different emissive species as aggregates. In previous studies, partially overlapped (~390 nm) and fully overlapped (~420 nm) emission bands were attributed to the formation of excimers when the carbazole units interact [55] [–] [58]. Therefore, the same analogy could be done for the carbazole derivatives **2** and **3**; while the lower energy emission (~530 nm) could be associated with partially overlapped aggregates, the fully overlapped ones are presented at higher energy (~430 nm). In this way, the broad distribution of intermolecular packing of the formed films could enhance the formation of different electroluminescent species as can be observed in the performed OLED devices.

4. Conclusions

The photophysical properties of a series of star-shaped molecules decorated with TPA and carbazole groups in the periphery have been studied here. All of them share 1,3,5-tristyrylbenzene as structural leitmotif in the molecular core which is a model fluorophore used in many spectroscopic studies. Despite the structural similarities between the three structures, their ultimate optoelectronic properties are different allowing us to compare and establish the role of peripheral TPA and carbazole groups. In general, all the compounds are highly fluorescent in solution, with higher quantum yields for compound **1** (Φ_F = 77–91%) and somewhat lower for compound **3** (Φ_F = 47–67%). The photoexcitation of the studied compounds leads to ICT transitions and geometrical modifications involving a single branch of the molecule. The largest change in the dipole moment upon photoexcitation, as well as the highest Δr index, were found for compound **1**. The strong ICT character of the photoexcitation of **1**, associated to its higher molecular flexibility, leads to a greater planarization in the excited state enhancing its fluorescence emission. The lifetime of the excited state of **1** also increases upon increasing the solvent polarity. On the other hand, the relationship observed between the non-radiative rate constant of **3** and the solvent viscosity was attributed the higher rigidity of its molecular

structure because the carbazole groups are more embedded in the branches of the molecule. Thus, the viscous media hinder non-radiative deactivation mechanisms of compound **3** such as the *trans-cis* photoisomerization and IC. Compound **2**, despite having a carbazole, is bound by the nitrogen atom which confers some freedom of movement, and its behavior is intermediate to compounds **1** and **3**.

To further probe the possibility of implementing those molecules on solid state lighting, a proof of concept of light-emitting devices was fabricated for the synthetized compounds. The results highlight the importance of the molecule structure not only on the photophysical performance, but the molecule design also plays an important role in the aggregation behavior, ending in a different device performance.

Author contributions

A.G.R., A.N. and J.C.G.M. conceived the idea and designed the experiments. J.T. synthetized compounds 1–3. P.J.P.L. carried out the spectroscopic experiments in solution. C.M. and J.H. performed the spectroscopic experiments and electroluminescence measurements in solid state. M.M. and A.N. carried out the DFT calculations on compounds 1–3. All authors contributed to the results discussions and are in agreement with the results. A.G.R., A.N., J.C.G.M, C.M. and I.B. contributed to writing the manuscript.

Declaration of competing interest

The authors declare that they have no known competing financial interests or personal relationships that could have appeared to influence the work reported in this paper.

Acknowledgments

This work is supported by the “Ministerio de Economía, Industria y Competitividad” of Spain through Project CTQ2017-84561-P. The authors would also like to thank the ’Universidad de Castilla-La Mancha’ for financially supporting the research described in this article (Project 2019-GRIN-27175). J. Pacheco-Liñán thanks the ’Junta de Comunidades de Castilla-La Mancha’ for his postdoctoral fellowship [2018/15132]. Computation study was financially supported by ’Junta de Andalucía (Consejería de Transformación Económica, Industria, Conocimiento y Universidades); FQM-337’ and ’Universidad de Jaén’ (Acción 1).

Appendix A. Supplementary data

Supplementary data to this article can be found online at https://doi.org/10.1016/j.dyepig.2022.110105.

References

[1] Schmidt AW, Reddy KR, Knölker HJ. Occurrence, biogenesis, and synthesis of biologically active carbazole alkaloids. Chem Rev 2012;112:3193–328.
[2] Devadiga D, Selvakumar M, Shetty P, Santosh M, Chandrabose RS, Karazhanov S. Recent developments in metal-free organic sensitizers derived from carbazole, triphenylamine, and phenothiazine for dye-sensitized solar cells. Int J Energy Res 2021;45:6584–643.
[3] Wex B, Kaafarani BR. Perspective on carbazole-based organic compounds as emitters and hosts in TADF applications. J Mater Chem C 2017;5:8622–53.
[4] Ledwon P. Recent advances of donor-acceptor type carbazole-based molecules for light emitting applications. Org Electron 2019;75:105422.
[5] Murakami TN, Koumura N. Development of next-generation organic-based solar cells: studies on dye-sensitized and perovskite solar cells. Adv Energy Mater 2019;9:1802967.
[6] Dumur F. Carbazole-based polymers as hosts for solution-processed organic light-emitting diodes: simplicity, efficacy. Org Electron 2015;25:345–61.
[7] Liu Y, Pang L, Liu T, Guo J, Wang J, Li W. Novel triphenylamine polyazomethines bearing carbazole and trifluoromethyl substituents: preparation and electrochromic behavior. Dyes Pigments 2020;173:107921.
[8] Liu Y, Liu T, Pang L, Guo J, Wang J, Qi D, et al. Novel triphenylamine polyamides bearing carbazole and aniline substituents for multi-colored electrochromic applications. Dyes Pigments 2020;173:107995.
[9] Sánchez-Ruiz A, Sousa-Herves A, Tolosa J, Navarro A, García-Martínez JC. Aggregation-induced emission properties in fully π-conjugated polymers, dendrimers, and oligomers. Polymers (Basel) 2021;13:1–49.
[10] Qiu J, Wang K, Lian Z, Yang X, Huang W, Qin A, et al. Prediction and understanding of AIE effect by quantum mechanics-aided machine-learning algorithm. Chem Commun 2018;54:7955–8.
[11] Lin HT, Huang CL, Liou GS. Design, synthesis, and electrofluorochromism of new triphenylamine derivatives with AIE-active pendent groups. ACS Appl Mater Interfaces 2019;11:11684–90.
[12] feng Yao L, long Huang X, ying Xia H, feng He H, Shen L. Triphenylamine or carbazole-containing dibenzothiophene sulfones: color-tunable solid-state fluorescence and hypso- or bathochromic mechanofluorochromic behaviors. Dyes Pigments 2021;184:108747.
[13] Grigoras M, Vacareanu L, Ivan T, Catargiu AM. Photophysical properties of isoelectronic oligomers with vinylene, imine, azine and ethynylene spacers bearing triphenylamine and carbazole end-groups. Dyes Pigments 2013;98:71–81.
[14] Chan CYK, Lam JWY, Zhao Z, Chen S, Lu P, Sung HHY, et al. Aggregation-induced emission, mechanochromism and blue electroluminescence of carbazole and triphenylamine-substituted ethenes. J Mater Chem C 2014;2:4320–7.
[15] Domínguez R, Moral M, Fernández-Liencres MP, Peña-Ruiz T, Tolosa J, Canales-Vázquez J, et al. Understanding the driving mechanisms of enhanced luminescence emission of oligo(styryl)benzenes and tri(styryl)- s -triazine. Chem – A Eur J 2020;26:3373–84.
[16] Moral M, Tolosa J, Canales-Vázquez J, Sancho-García JC, Garzón-Ruiz A, García-Martínez JC. Combined theoretical and experimental study on intramolecular charge transfer processes in star-shaped conjugated molecules. J Phys Chem C 2019;123:11179–88.
[17] Garzón A, Fernández-Liencres MP, Moral M, Peña-Ruiz T, Navarro A, Tolosa J, et al. Effect of the aggregation on the photophysical properties of a blue-emitting star-shaped molecule based on 1,3,5-tristyrylbenzene. J Phys Chem C 2017;121:4720–33.
[18] Uda M, Momotake A, Arai T. 1,3,5-Tristyrylbenzene dendrimers: a novel model system to explore oxygen quenching in a highly organized environment. Org Biomol Chem 2003;1:1635.
[19] Meier H, Zertani R, Noller K, Oelkrug D, Krabichler G. Fluoreszenz-untersuchungen an styrylsubstituierten benzolen. Chem Ber 1986;119:1716–24.
[20] Winter W, Langjahr U, Meier H, Merkuschew J, Juriew J. Photochemie des 1,3,5-Tristyrylbenzols. Chem Ber 1984;117:2452–63.
[21] Coya C, de Andrés A, Gómez R, Seoane C, Segura JL. On the blue emission of a novel solution-processed stilbenoid dendrimer thin film for OLED displays. J Lumin 2008;128:761–4.
[22] Coya C, De Andrés A, Zaldo C, Lvarez AL, Arredondo B, Gómez R, et al. Full-solution-processed blue organic light emitting device based on a fluorescent 1,3,5-tristyrylbenzene stilbenoid small molecule. J Appl Phys 2009;105:044510.
[23] Yan Z-Q, Xu B, Dong Y-J, Tian W-J, Li A-W. The photophysical properties and two-photon absorption of novel triphenylamine-based dendrimers. Dyes Pigments 2011;90:269–74.
[24] Frisch MJ, Trucks GW, Schlegel HB, Scuseria GE, Robb MA, Cheeseman JR, et al. Gaussian 16, revision D.01. Wallingford CT: Gaussian, Inc; 2009. 2009.
[25] Zhao Y, Truhlar DG. The M06 suite of density functionals for main group thermochemistry, thermochemical kinetics, noncovalent interactions, excited states, and transition elements: two new functionals and systematic testing of four M06-class functionals and 12 other function. Theor Chem Acc 2008;120:215–41.
[26] Moral M, Domínguez R, Fernández-Liencres MP, Garzón-Ruiz A, García-Martínez JC, Navarro A. Photophysical features and semiconducting properties of propeller-shaped oligo(styryl)benzenes. J Chem Phys 2019;150:064309.
[27] Cossi M, Rega N, Scalmani G, Barone V. Energies, structures, and electronic properties of molecules in solution with the C-PCM solvation model. J Comput Chem 2003;24:669–81.
[28] Tomasi J, Mennucci B, Cammi R. Quantum mechanical continuum solvation models. Chem Rev 2005;105:2999–3094.
[29] Cammi R, Corni S, Mennucci B, Tomasi J. Electronic excitation energies of molecules in solution: state specific and linear response methods for nonequilibrium continuum solvation models. J Chem Phys 2005;122:104513.
[30] Improta R, Barone V, Scalmani G, Frisch MJ. A state-specific polarizable continuum model time dependent density functional theory method for excited state calculations in solution. J Chem Phys 2006;125:054103.
[31] Scalmani G, Frisch MJ, Mennucci B, Tomasi J, Cammi R, Barone V. Geometries and properties of excited states in the gas phase and in solution: theory and application of a time-dependent density functional theory polarizable continuum model. J Chem Phys 2006;124:094107.
[32] Reimers JR. A practical method for the use of curvilinear coordinates in calculations of normal-mode-projected displacements and Duschinsky rotation matrices for large molecules. J Chem Phys 2001;115:9103–9.
[33] Guido CA, Cortona P, Mennucci B, Adamo C. On the metric of charge transfer molecular excitations: a simple chemical descriptor. J Chem Theor Comput 2013;9:3118–26.
[34] Kertész M. Bond length alternation and energy gap in (CH)x. Application of the intermediate exciton formalism. Chem Phys 1979;44:349–56.
[35] Brédas JL. Relationship between band gap and bond length alternation in organic conjugated polymers. J Chem Phys 1985;82:3808–11.
[36] Jacquemin D, Adamo C. Bond length alternation of conjugated oligomers: wave function and DFT Benchmarks. J Chem Theor Comput 2011;7:369–76.
[37] Díez-Barra E, García-Martínez JC, Merino S, del Rey R, Rodríguez-López J, Sánchez-Verdú P, et al. Synthesis, characterization, and optical response of dipolar

and non-dipolar poly(phenylenevinylene) dendrimers. J Org Chem 2001;66:5664–70.
[38] Lippert E. Spektroskopische Bestimmung des Dipolmomentes aromatischer Verbindungen im ersten angeregten Singulettzustand. Zeitschrift Für Elektrochemie. Berichte Der Bunsengesellschaft Für Phys Chemie 1957;61:962–75.
[39] Mataga N, Kaifu Y, Koizumi M. Solvent effects upon fluorescence spectra and the dipolemoments of excited molecules. Bull Chem Soc Jpn 1956;29:465–70.
[40] Lakowicz JR. Principles of fluorescence spectroscopy. third ed. New York: Springer; 2006.
[41] Yuan WZ, Gong Y, Chen S, Shen XY, Lam JWY, Lu P, et al. Efficient solid emitters with aggregation-induced emission and intramolecular charge transfer characteristics: molecular design, synthesis, photophysical behaviors, and OLED application. Chem Mater 2012;24:1518–28.
[42] Eom YK, Hong JY, Kim J, Kim HK. Triphenylamine-based organic sensitizers with π-spacer structural engineering for dye-sensitized solar cells: synthesis, theoretical calculations, molecular spectroscopy and structure-property-performance relationships. Dyes Pigments 2017;136:496–504.
[43] Köhler A, Bässler H. Electronic processes in organic semiconductors. Weinheim, Germany: Wiley-VCH Verlag GmbH & Co. KGaA; 2015.
[44] Schneider S, Brem B, Jäger W, Rehaber H, Lenoir D, Frank R. Influence of solvent viscosity on the photoisomerization of a novel trans-stilbene derivative with hindered single bond torsion. Chem Phys Lett 1999;308:211–7.
[45] Brey LA, Schuster GB, Drickamer HG. High-pressure study of the effect of viscosity on fluorescence and photoisomerization of trans-stilbene. J Am Chem Soc 1979;101:129–34.
[46] Saltiel J, D'Agostino JT. Separation of viscosity and temperature effects on the singlet pathway to stilbene photoisomerizaiion. J Am Chem Soc 1972;94:6445–56.
[47] Fischer G, Seger G, Muszkat KA, Fischer E. Emissions of statically hindered stilbene derivatives and related compounds. Part IV. Large conformational differences between ground and excited states of sterically hindered stilbenes: implications regarding Stokes shifts and viscosity or temperature de. J Chem Soc Perkin Trans 1975;2:1569–76.
[48] CRC handbook of chemistry and physicsLide DR, editor. J Am Chem Soc 2007;129.724–724.
[49] Angulo G, Brucka M, Gerecke M, Grampp G, Jeannerat D, Milkiewicz J, et al. Characterization of dimethylsulfoxide/glycerol mixtures: a binary solvent system for the study of "friction-dependent" chemical reactivity. Phys Chem Chem Phys 2016;18:18460–9.
[50] Reichardt C. Solvatochromic dyes as solvent polarity indicators. Chem Rev 1994;94:2319–58.
[51] Granadino-Roldán JM, Garzón A, Moral M, García G, Peña-Ruiz T, Paz Fernández-Liencres M, et al. Theoretical estimation of the optical bandgap in a series of poly(aryl-ethynylene)s: a DFT study. J Chem Phys 2014;140:044908.
[52] Juriew J, Skorochodowa T, Merkuschew J, Winter W, Meier H. A simple route to a new type of cyclophane. Angew Chem Int Ed Engl 1981;20:269–70.
[53] de Moraes IR, Scholz S, Hermenau M, Tietze ML, Schwab T, Hofmann S, Gather MC, Leo K. Impact of temperature on the efficiency of organic light emitting diodes. Org Electron 2015;26:158–63.
[54] Sah C, Noyce R, Shockley W. Carrier generation and recombination in P-N junctions and P-N junction characteristics. Proc IRE 1957;45:1228–43.
[55] Rommens J, Vaes A, Van der Auweraer M, De Schryver FC, Bässler H, Vestweber H, et al. Dual electroluminescence of an amino substituted 1,3,5-triphenylbenzene. J Appl Phys 1998;84:4487–94.
[56] Johnson GE. Spectroscopic study of carbazole by photoselection. J Phys Chem 1974;78:1512–21.
[57] Ghosh D, Chattopadhyay N. Characterization of the excimers of poly(N-vinylcarbazole) using TRANES. J Lumin 2011;131:2207–11.
[58] de Jong F, Daniels M, Vega-Castillo L, Kennes K, Martín C, de Miguel G, et al. 5,10-Dihydrobenzo[a]indolo[2,3- c]carbazoles as Novel OLED Emitters. J Phys Chem B 2019;123:1400–11.